Electromagnetic Performance of Rice Husk Ash

Shu-Ting Liu,[a] Xue-Gang Chen,[a,b,*] Ao-Bo Zhang,[a] Kang-Kang Yan,[a] and Ying Ye [a]

In this study, the electromagnetic (EM) performance of rice husk ash (RHA) calcined from rice husk was evaluated. Porous RHA with a bulk density of 0.4 g cm^{-3} is mainly composed of carbon and silica. The degrees of surface melting and destruction of porous structure increase with ashing temperature, while a nitrogen atmosphere retards surface melting and destruction because of the retention of carbon. A temperature of 700 ^{o}C is the lower limit for achieving significant surface melting, whereas 800 ^{o}C in air will destroy the porous structure and conductive network formed by surface melting. All RHA samples showed low permeability values caused by the absence of magnetic components. Sufficient conductive carbon and the formation of conductive networks are prerequisites for reasonable complex permittivity values. The calculated EM wave absorption of RHA achieved a maximum reflection loss (RL) of −21 dB at 2 to 18 GHz, including 5 GHz with an RL < −10 dB, which is above the average of traditional absorbers. This study reveals a new approach for fabricating an EM wave (microwave) absorber with low density and strong absorption by using agricultural wastes as starting materials.

Keywords: Rice hull; Microwave absorption; Permittivity; Reflection loss; Agricultural waste

*Contact information: a: Ocean College, Zhejiang University, Hangzhou, 310058, PR China; b: State Key Laboratory of Satellite Ocean Environment Dynamics, Second Institute of Oceanography, State Oceanic Administration, Hangzhou, 310012, PR China; *Corresponding author: chenxg83@zju.edu.cn*

INTRODUCTION

With the extensive exploitation of electromagnetic (EM) waves in modern technology, many problems concerning EM interference and pollution have emerged. Therefore, EM wave absorbers are in increasing demand in many civil and military fields, either to protect human beings from EM wave irradiation or to prevent military equipment from being detected by radar waves (Zhou *et al.* 2010; Hou *et al.* 2013; Drmota *et al*. 2012; Chen *et al*. 2011b). Ideal EM wave absorbers are light-weight, with strong absorption and broad bandwidth for EM wave absorption on the basis of thin matching thickness (Drmota *et al*. 2012; Chen *et al*. 2011b; Park *et al*. 2006). Many studies have been conducted in the pursuit of this target, most of which are focused on materials based on electric loss, magnetic loss, or a combination of both. Electric loss absorbers such as polymers (Ruckenstein and Park 1991), carbon fibers (Luo and Chung 1999), carbon nanotube (Wu *et al*. 2011; Yang and Gupta 2005), SiC fibers (Ding *et al*. 2013), and so on exhibit advantages such as low density, high strength, and high temperature resistance. However, their poor absorption and narrow bandwidth for EM waves restrict their practical applications (Chen *et al*. 2011b). However, magnetic loss absorbers including ferrite (Roy and Bera 2009; Suigimoto *et al*. 2005), carbonyl iron (Cheng *et al*. 2010), metallic powders (Gong and Zhen 2009), and so on show excellent EM wave absorption performance, but their high density constrains their applications in

military equipment, especially in aircraft (Moučka *et al*. 2007; Yoshida *et al*. 1999). Composites with a combination of both electric loss and magnetic loss such as FeCo/C nanocapsules (Han *et al*. 2009) and Fe/C nanocomposites (Zhao *et al*. 2009; Chen *et al*. 2012b; Chen *et al*. 2012c) incorporate the features of both traditional electric loss and magnetic loss materials, showing mediocre mechanical and EM wave absorption performance. Furthermore, many researchers have fabricated novel structures such as plasmonic (Hibbins *et al*. 2006), honeycomb structures (Chambers and Tennant 1994), and high-impedance surface absorbers (Sievenpiper *et al*. 1999) for EM wave absorption. However, these structures are limited by their poor mechanical performance or high cost. Therefore, EM wave absorbers remain a global concern.

Rice husk is the milling byproduct of rice and is usually treated as an agricultural waste to be burnt in open fields, which causes environmental problems. Rice husk contains 70 to 85% organic substance and the inorganic remainder consists mostly of silica (Givi *et al*. 2010; Yalçın and Sevinç 2000). Because of its abundance and low cost, many efforts have been made to transform rice husk from an environmental concern into a useful resource, taking into consideration its abundant carbon and silica contents. For instance, the chemical composition and insulation performance of rice husk make it possible to act as a building material (Ismail and Waliuddin 1996; Memon *et al*. 2011) or a filler to enhance the mechanical properties of mortar, concrete (Givi *et al*. 2010), and polymers (Kord 2011; Rahman *et al*. 2010). On the other hand, rice husk is an important precursor for adsorbers (Che Man *et al*. 2012) and catalyst carriers because of its low cost and porous structure after ashing (Chen *et al*. 2010; Chandrasekhar *et al*. 2003; Lv *et al*. 2009). As for EM wave absorption, Nornikman *et al*. (2009, 2010) examined the microwave absorption of rice husk in pyramidal form, while Liu *et al*. (2004) investigated the EM shielding of carbonized rice husk and its magnetic composites at 30 to 1500 MHz. Nevertheless, no work has been done to study the EM parameters of rice husk ash (RHA), especially their relationship with the physical-chemical characteristics of RHA.

In this study, the EM performance of RHA ashed under different atmospheres and temperatures was evaluated. The experiments were carried out to examine variations in the physicochemical characteristics of RHA, determine the corresponding complex permittivity and permeability values, and further calculate the frequency dependence of reflection loss (RL) for EM waves at 2 to 18 GHz. The results confirmed the potential of RHA as an alternative EM wave absorber.

EXPERIMENTAL

Materials

Rice husk was obtained from Quzhou, Zhejiang province. It was washed thoroughly with deionized water to remove impurities and dried at 60 ^{o}C before usage. The average chemical composition of rice husk is 79.6% organic substances, 19.02% SiO_2, 0.7% K_2O, 0.28% CaO, 0.14% MgO, 0.13% P_2O_5, 0.06% S, 0.04% Cl, and 0.03% other materials.

Preparation of Rice Husk Ash

A certain amount (50 g) of rice husk was calcined in a furnace at 400, 500, 600, 700, and 800 ^{o}C for 2 h, respectively. The heating rate was 10 ^{o}C min^{-1} for all samples.

After being cooled to room temperature, rice husk ash (RHA) samples were obtained and were labeled A400 to A800 (ashed in air) or N400 to N800 (ashed in nitrogen), respectively, according to ashing temperature and atmosphere.

Characterization

The phase purity and crystal structure of the samples were determined by a D/max 2550 X-ray diffractometer (XRD) (Rigaku, Japan) with Cu Kα radiation (λ=0.15406 nm) at a scan rate of 0.02° s^{-1}. The operation voltage and current were maintained at 36 kV and 34 mA, respectively. The surface morphologies were observed by a 650 FEG field emission scanning electronic microscope (FE-SEM) (Quanta, USA) at an accelerating voltage of 10 to 20 kV. The chemical compositions of the samples were studied by an S-4800 energy dispersive spectrometer (EDS) (Hitachi, Japan) at an accelerating voltage of 25.0 kV. Surface area and pore characteristics of the samples were measured by nitrogen adsorption and desorption at 77 K using a Coulter OMNISORP surface and pore analyzer. The EM parameters were examined with a HP8720ES vector network analyzer (Agilent, USA) using the T/R coaxial line method at an EM wave frequency of 2 to 18 GHz and a thickness of 2 mm, using paraffin as substrate. The filling rates were 30% for all measurements. The relative complex permittivity ($\varepsilon = \varepsilon' - j\varepsilon''$) and permeability ($\mu = \mu' - j\mu''$) were calculated using the measured T/R coefficients. The measurement errors were less than 10% when $\varepsilon' < 15$. The resistivity values of RHA were determined by a KDY-1 four-probe resistivity meter with an input current of 0.005 mA. Bulk densities of RHA were determined using the following method: a 50-mL cylinder was filled to a specified volume with samples that had been dried in an oven at 80 °C overnight. The cylinder was tapped for at least 1 to 2 min to compact the samples, then weighed. The bulk density was calculated as:

$$\text{Bulk density (g cm}^{-3}\text{)} = \text{weight of sample (g)/volume of packed sample (cm}^{3}\text{)} \quad (1)$$

RESULTS AND DISCUSSION

XRD and SEM Characterizations

The chemical compositions and crystal structures of RHA may play important roles in determining their EM properties because the dielectric loss of carbon is generally higher than that of silica (Cheng *et al*. 2012). Figure 1 shows the XRD patterns of RHA samples prepared under different temperatures and atmospheres. All samples exhibited a broad band at approximately 2θ = 22°, which is the characteristic peak of amorphous silica. The sharpness of this peak generally increased with ashing temperature, suggesting the temperature-dependent crystallization of silica. A small peak corresponding to carbon was observed at 2θ = 28° for all samples. The intensities of this peak of RHA ashed in nitrogen were slightly higher than those ashed in air, which was caused by the preservation of carbon under an inert atmosphere. The XRD analyses indicate the amorphous nature of all RHA samples ashed both in air and nitrogen.

According to our previous study (Chen *et al*. 2011a), the carbon content of A400-A800 decreased with ashing temperature from about 40% at 400 ^{o}C to less than 3% at 800 ^{o}C because of the continuous degradation of organic matters in rice husk, while the silica content simultaneously increased from 30% to more than 95%. Conversely, RHA

ashed in nitrogen generally showed invariant carbon (about 60%) and silica (about 35%) contents because of the retention of carbon.

The corresponding SEM images of RHA samples are presented in Fig. 2. The surface features of RHA samples varied with ashing temperature and atmosphere. When calcined at relatively low temperatures of less than 600 ^{o}C, the obtained samples A500 and N400 preserved the cob-shaped cellulose structure of raw rice husk (Chen *et al*. 2011a), indicating that only minor thermal destruction occurred under low temperatures. When the ashing temperature was increased to 800 ^{o}C, however, ashing atmosphere played a key role in shaping the obtained RHA samples.

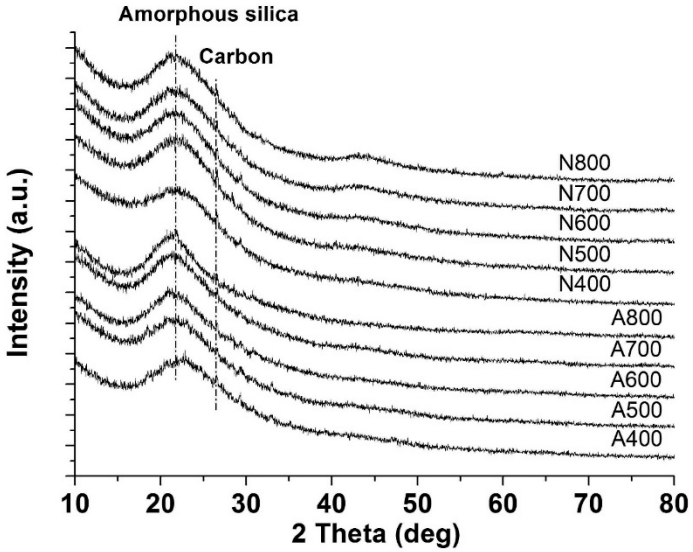

Fig. 1. XRD patterns of rice husk ash samples

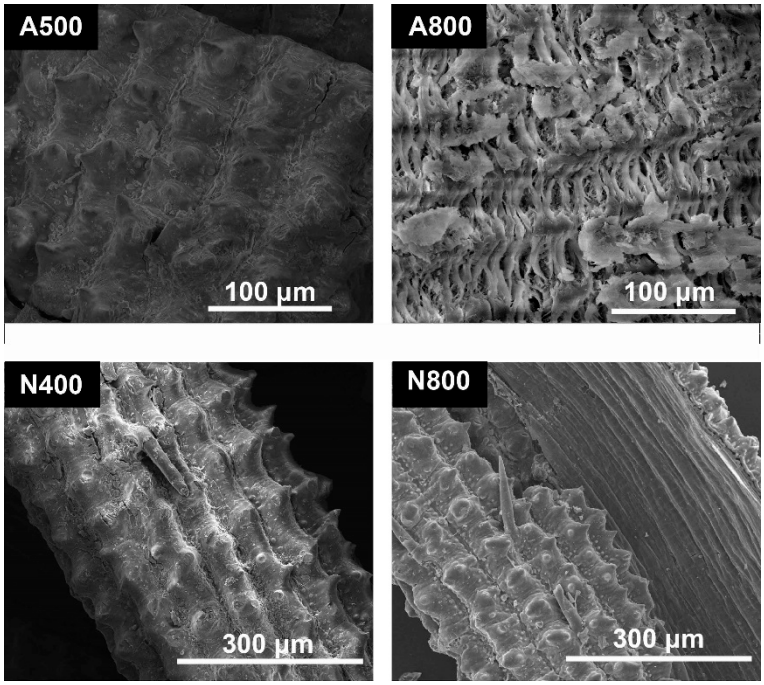

Fig. 2. SEM images of selected rice husk ash samples: A500, A800, N400, and N800

Because of the enhanced thermal destruction of organic matter in rice husk, A800 that was ashed at 800 °C in an air atmosphere showed a porous structure with a cross-linked heat-refractory silica framework. N800 that ashed in nitrogen, however, preserved the original structure of raw rice husk, which was comparable to that of N400 and A500. This is attributed to the fact that the organic matters in rice husk will be carbonized to amorphous carbon rather than carbon gases under nitrogen atmosphere. The retained carbon retarded the thermal destruction and consequently preserved the original structure. In addition, A500, N400, and N800 showed preserved needle-like protuberances because the refractory silica was mainly localized in regions corresponding to the protrusions and adjoining sloping areas (Park *et al*. 2003; Chakraborty *et al*. 2011).

BET Surface Area and Pore Analyses

The BET surface area and pore size distribution may affect the EM wave absorption of RHA samples via the scattering effect (Chen *et al*. 2011b). As shown in Fig. 3 (a, b), the adsorption and desorption curves of A400-A800 belong to type IV isotherms for their characteristic hysteresis loops, whereas the samples that had been ashed under nitrogen showed type I isotherms characterized by a nearly horizontal plateau and a "tail" near the saturation pressure (Chen *et al*. 2011a). The curves of N400 were almost parallel the pressure axis with low adsorption volumes, indicating poorly developed pores. The curves of N700, N600, and N500 were not closed, which may be attributed to the presence of micropores (< 2 nm).

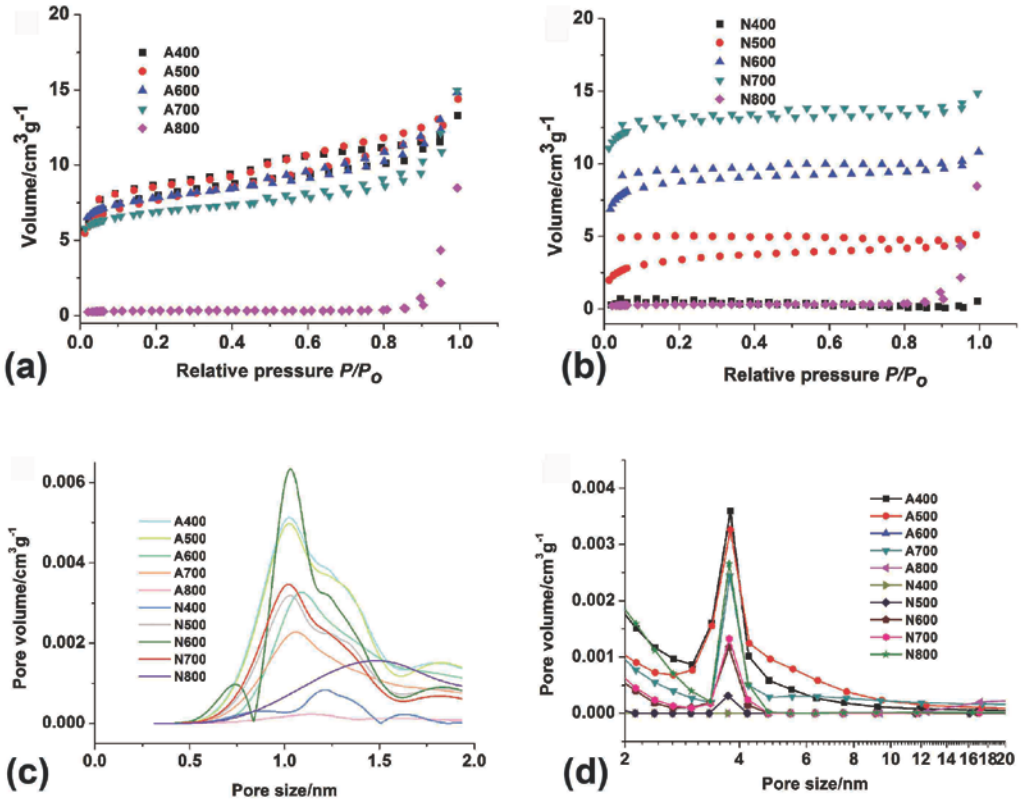

Fig. 3. (a, b) Nitrogen adsorption and desorption curves and (c) micropore and (d) mesopore (2 - 50 nm) size distributions of rice husk ash samples

Table 1 shows the calculated BET surface areas and pore volumes of RHA samples. Thermal destruction was enhanced as temperature increased, while a nitrogen atmosphere preserved the carbon in RHA. On the other hand, pores are blocked by surface melting as calcination proceeds (Chen *et al*. 2011a). Therefore, micropore volume and the mesopore volume of A400-A800 increased with ashing temperature at first and then sharply declined because micropores and mesopores were blocked one after another as surface melting was enhanced, whereas that of N400-N800 increased with temperature continuously because of the retention of carbon. Accordingly, the BET surface area and total pore volume exhibited the same trends as micropore and mesopore volumes, and the mesopore fraction and average pore size generally increased with ashing temperature. The mesopore volume, mesopore fraction, and average pore size of N400-N800 were significantly lower than that of A400-A800 because of the preservation of carbon. All samples except N400 and N800 displayed similar maximum micropore volumes at 1.0 to 1.1 nm and maximum mesopore volumes at 3.7 nm (Fig. 3c, d), which can be attributed to the hierarchical distribution of silica framework (Chen *et al*. 2011a). Note that the BET surface area and pore volumes of A800 are much lower than those of A700, while the average pore size is tenfold higher, indicating that the porous structure of A800 had collapsed.

Table 1. BET Surface Areas and Pore Volumes of RHA Samples

Samples	BET surface area/m^2g^{-1}	Total pore volume/ cm^3g^{-1}	Micropore volume/ cm^3g^{-1}	Mesopore volume/ cm^3g^{-1}	Mesopore fraction/%	Average pore size/nm
A400	241.1	0.1761	0.1026	0.0701	39.80	2.9
A500	234.7	0.1900	0.0979	0.0878	46.21	3.2
A600	247.3	0.2198	0.1135	0.1088	49.51	3.6
A700	184.9	0.1890	0.0855	0.0912	48.24	4.1
A800	10.1	0.1241	0.0047	0.0858	69.17	49.1
N400*	15.7	0.0080	0.0064	0.0023	29.02	2.0
N500	114.1	0.0622	0.0395	0.0037	6.01	2.2
N600	220.1	0.1222	0.0968	0.0122	9.96	2.2
N700	254.7	0.1384	0.1181	0.0146	10.52	2.2
N800	324.3	0.1855	0.1576	0.0221	11.89	2.3

* The values for N400 may not correct due to its abnormal adsorption-desorption curves.

Permittivity and Permeability

The frequency dependence of EM parameters of RHA samples were detected using a vector network analyzer at a range of 2 to 18 GHz. As shown in Fig. 4, most samples except A700, N700, and N800 showed relatively constant low relative complex ε values with ε' of 2.5 to 3 and ε'' of 0 to 0.3. Consequently, their dielectric loss tangents ($\tan \delta_e = \varepsilon''/\varepsilon'$) were generally invariant at 0 to 0.05. A700, N700, and N800 exhibited much higher complex permittivity, where the ε' values (between 7 and 16) generally decreased with frequency while their ε'' values (from 1 to 6) and tan δ_e (higher than 0.1)

increase. The ε and tan δ_e values of N800 presented some fluctuations as a function of frequency and showed maxima at about 9 GHz.

There are many factors that may affect the permittivity of RHA samples. According to the free electron theory, ε'' is approximately equal to $\sigma/ 2\pi\varepsilon_o f$, where σ is the conductivity of the sample; that is, higher ε'' values require higher conductivities (or lower resistivity). In this study, analyses that failed to obtain resistivity values for most samples may be ascribed to limitation of measurement range. Nevertheless, resistivity for N700 and N800 was successfully obtained, and the values were between $4*10^4$ and $1.5*10^5$ Ω. Although the results may not be accurate because of the constraint of the sampling method, which may cause tenfold errors, these results indicate that higher ashing temperatures will cause higher conductivities through the conductive network formed by surface melting. Because most components in RHA have high melting points, the surface melting was mainly induced by the melting of K_2O (melting point: 770 ^oC) and its eutectic system with a melting point of lower than 770 ^oC. In this study, surface melting occurred only at ashing temperatures greater than 700 ^oC such that a conductive network was successfully formed and complex permittivity was enhanced. Ashing temperatures of lower than 700 ^oC, however, were not sufficient to cause the surface melting and conductive network that are prerequisites for high permittivity values.

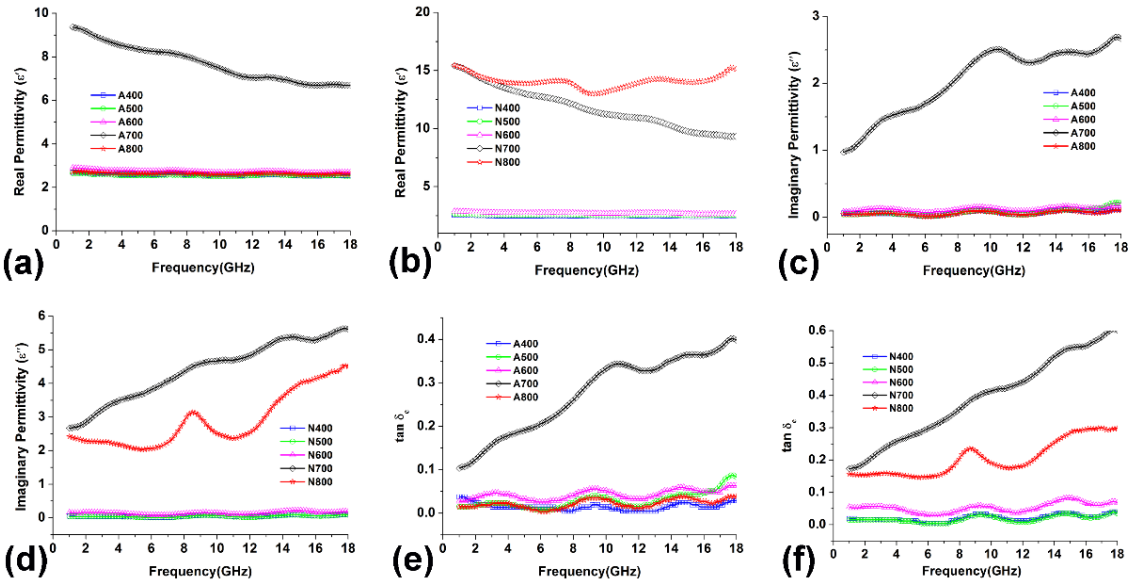

Fig. 4. Frequency dependence of (a, b) real permittivity, (c, d) imaginary permittivity, and (e, f) dielectric loss tangent of rice husk ash samples

Based on the above statement, A700, A800, N700, and N800 should show comparably high complex permittivity values. However, the ε values for A800 were significantly lower than that of others, while N700 and N800 exhibited higher ε values than that of A700. These phenomena are ascribed to two causes. First, the dielectric loss of carbon is much higher than that of silica for its charge migration and dipole polarization (Cheng *et al*. 2012). Therefore, N700 and N800 with higher carbon contents generally showed higher ε values. Second, the porous structure of A800 was collapsed according to its BET surface area and pore characteristics. The conductive network formed by surface melting was destroyed as well. Consequently, A800 presented much lower ε values than that of A700.

Figure 5 shows the frequency dependence of the relatively complex permeability of RHA samples. Because of the absence of magnetic components, all samples exhibited relatively constant μ' values of about 1 and μ'' values of 0 to 0.2, which are close to the values for air. All samples showed zigzag curves for μ'' values, which suggests high measurement errors. Nevertheless, all the μ'' values showed maximum values at 2 to 4 GHz and 16 to 18 GHz, respectively, which may be attributed to the eddy effect of EM waves in the absorber, that higher eddy currents will result in higher μ'' values (Chen *et al*. 2011b). Because RHA samples ashed in nitrogen contained much higher conductive carbon than those ashed in air, N400-N800 induced higher eddy effects for EM waves and therefore resulted in higher tan δ_m values. After all, the complex permittivity and permeability values suggest that the absorption of RHA for EM waves was mainly achieved by dielectric loss.

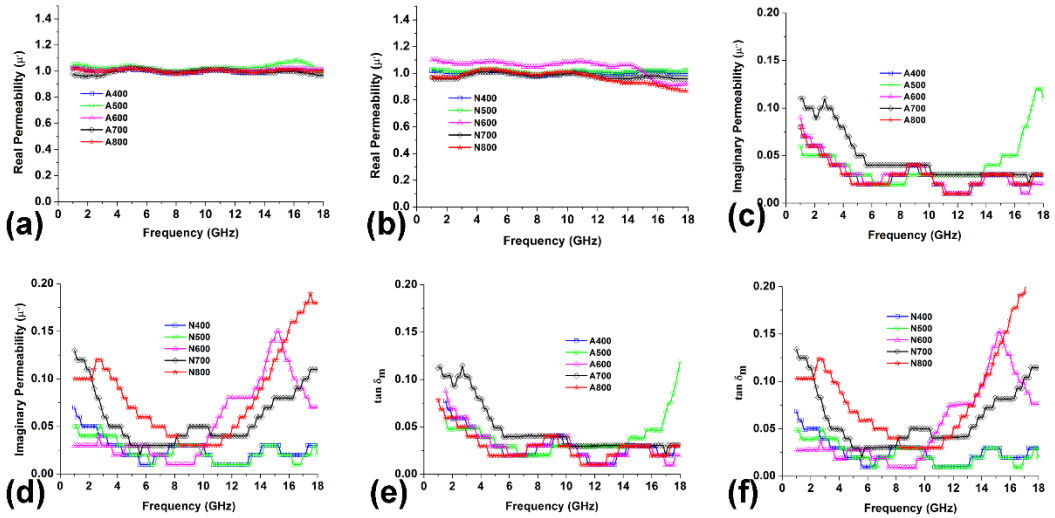

Fig. 5. Frequency dependence of (a, b) real permeability, (c, d) imaginary permeability, and (e, f) magnetic loss tangent of rice husk ash samples

EM Wave Absorption Performance

According to the transmission line theory, the RL of absorbers can be evaluated from the measured complex permittivity and permeability values using the following equations,

$$Z_{in} = Z_0\sqrt{\frac{\mu}{\varepsilon}}\tanh[\,j\frac{2\pi fd}{c}\sqrt{\mu\varepsilon}\,] \tag{2}$$

$$RL(dB) = 20\log\left|\frac{Z_{in}-Z_0}{Z_{in}+Z_0}\right| \tag{3}$$

where Z_{in} and Z_0 are the impedances of the absorber and air, respectively. ε and μ are the complex permittivity and permeability of absorber, respectively, f is the frequency of EM wave, d is the thickness of the absorber, and c is the velocity of light. As shown in Fig. 6, the calculated RL of most samples were less than 3 dB for all frequencies because of their low dielectric loss and magnetic loss for EM waves. Because A700, N700, and N800 presented significantly higher dielectric loss tangents, they showed considerable absorption for EM waves. The maximum RLs of A700, N700, and N800 were −21 dB,

−18.9 dB, and −12.5 dB, respectively, which are reliable for achieving > 90% absorption for EM waves. The bandwidth of RL < −5 dB for A700, N700, and N800 were 7 GHz, 9.2 GHz, and 4.4 GHz, respectively, while those for RL < −10 dB were 5 GHz, 3.5 GHz, and 1.9 GHz, respectively. When compared with traditional EM wave absorbers (Table 2), RHA is a potential absorber with many advantages. First, the obtained RHA samples were relatively low in bulk density (only about 0.4 g cm^{-3}). Bulk density is of great importance for the practical application of EM wave absorbers, especially in military fields. Second, RHA showed considerable absorption for EM waves without the addition of magnetic materials. The maximum RL and bandwidth of RL < −5 dB and RL < −10 dB of RHA were above the average of traditional absorbers. Third, this study utilized low-cost agricultural waste that is usually abandoned and therefore transformed agricultural waste from trash to treasure.

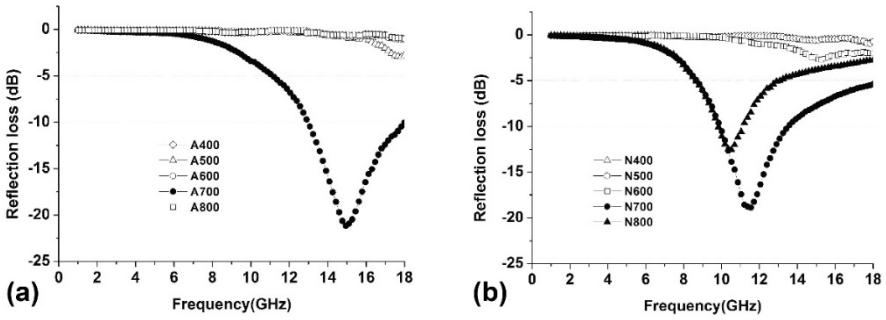

Fig. 6. Frequency dependence of reflection loss of rice husk ash samples for EM waves

Table 2. Comparisons between the EM Wave Absorption Performance of Rice Husk Ash in This Study and Traditional EM Wave Absorbers

Samples	Bulk density (g cm^{-3})	Thickness (mm)	Bandwidth of RL<−5 dB	Bandwidth of RL<−10 dB	Maximum RL (dB)
A700	0.37	2.0	7.0	5.0	−21.0
N700	0.38	2.0	9.2	3.5	−18.9
N800	0.40	2.0	4.4	1.9	−12.5
Porous carbon fiber (Guan *et al*. 2007)	1.28	2.9	/	10.9	−15.5
Porous Fe (Chen *et al*. 2012a)	0.53	2.0	4.6	2.2	−21.9
Co-Fe film (Kim *et al*. 2004)	0.8	1.5	/	4.0	−18.0
Carbonyl Iron/Rubber (Sievenpiper *et al*. 1999)	2.9*	1.8	/	8.5	−37.4
* Calculated according to the mass fractions and bulk densities of carbonyl Iron and rubber					

CONCLUSIONS

1. The rice husk ash (RHA) microwave absorber in this study, which utilized abundant and low-cost agricultural waste as a raw material, is low in bulk density (less than 0.4 g cm^{-3}). With advantages such as high EM wave absorption, low density, low cost, and environmental friendliness, RHA is a promising light-weight EM wave absorber.
2. Most samples show low permittivity values, while A700, N700, and N800, which were ashed at 700 and 800 ^{o}C, exhibit considerable permittivity values with ε' of more than 7, ε'' of higher than 1, and $\tan\delta_e$ of greater than 0.1.
3. The dielectric loss of RHA samples determine their absorption capacities for EM waves. A700, N700, and N800 exhibit considerable absorption for EM waves, while most samples show low RL values of less than 3 dB. The maximum RL, bandwidth of RL < −10 dB, and bandwidth of RL < −5 dB achieved by RHA were −21 dB, 5 GHz, and 9.2 GHz, respectively, which are above the average for traditional absorbers.

ACKNOWLEDGMENTS

This research was supported by the Research Fund for the Doctoral Program of Higher Education of China (20110101120045) and the programs for Zhejiang Leading Team of S&T Innovation (2010R50036).

REFERENCES CITED

Chakraborty, S., Chowdhury, S., and Saha, P. D. (2011). "Adsorption of crystal violet from aqueous solution onto NaOH-modified rice husk," *Carbohyd. Polym.* 86(4), 1533-1541.

Chambers, B., and Tennant, A. (1994). "Design of wideband Jaumann radar absorbers with optimum oblique incidence performance," *Electron. Lett*. 30(18), 1530-1532.

Chandrasekhar, S., Satyanarayana, K. G., Pramada, P. N., Raghavan, P., and Gupta, T. N. (2003). "Review processing, properties and applications of reactive silica from rice husk—An overview," *J. Mater. Sci*. 38(15), 3159-3168.

Che Man, H., Chin, W. H., Zadeh, M. R., and Yusof, M. R. M. (2012). "Adsorption potential of unmodified rice husk for boron removal," *BioResources* 7(3), 3810-3822.

Chen, X., Cheng, J., Lv, S., Zhang, P., Liu, S., and Ye, Y. (2012a). "Preparation of porous magnetic nanocomposites using corncob powders as template and their applications for electromagnetic wave absorption," *Compos. Sci. Technol.* 72(8), 908-914.

Chen, X., Lv, S., Ye, Y., Cheng, J., and Yin, S. (2010). "Preparation and characterization of rice husk/ferrite composites," *Chinese Chem. Lett.* 21(2), 122-126.

Chen, X., Lv, S., Zhang, P., Cheng, J., Liu, S., and Ye, Y. (2012b). "Fabrication and electromagnetic performance of micro-tubular nanocomposites composed of mono-disperse iron nanoparticles and carbon," *J. Magn. Magn. Mater*. 324(9), 1745-1751.

Chen, X., Lv, S., Zhang, P., Zhang, L., and Ye, Y. (2011a). "Thermal destruction of rice hull in air and nitrogen," *J. Therm. Anal. Calorim.* 104(4), 1055-1062.

Chen, X., Ye, Y., and Cheng, J. (2011b). "Recent progress in electromagnetic wave absorbers," *J. Inorg. Mater*. 26(5), 449-456.

Chen, X., Ye, Y., Lv, S., and Cheng, J. (2012c). "Preparation and microwave absorption of micro-fibrous Fe/C nanocomposite," *Funct. Mater. Lett.* 5(4), 1250036.

Cheng, E. M., Malek, F., Ahmed, M., You, K. Y., Lee, K. Y., and Nornikaman, H. (2012). "The use of dielectric mixture equations to analyze the dielectric properties of a mixture of rubber tire dust and rice husks in a microwave absorber," *Prog. Electromagn. Res.* 129, 559-578.

Cheng, Y. L., Dai, J. M., Wu, D. J., and Sun, Y. P. (2010). "Electromagnetic and microwave absorption properties of carbonyl iron/$La_{0.6}Sr_{0.4}MnO_3$ composites," *J. Magn. Magn. Mater.* 322(1), 97-101.

Ding, D., Shi, Y., Wu, Z., Zhou, W., Lou, F., and Chen, J. (2013). "Electromagnetic interference shielding and dielectric properties of SiC_f/SiC composites containing pyrolytic carbon interphase," *Carbon* 60, 552-555.

Drmota, A., Koselj, J., Drofenik, M., and Žnidaršič, A. (2012). "Electromagnetic wave absorption of polymeric nanocomposites based on ferrite with a spinel and hexagonal crystal structure," *J. Magn. Magn. Mater.* 324(6), 1225-1229.

Givi, A. N., Rashid, S. A., Aziz, F. N. A., and Salleh, M. A. M. (2010). "Contribution of rice husk ash to the properties of mortar and concrete: A review," *J. Am. Sci.* 6(3), 157-165.

Gong, Y. X., and Zhen, L. (2009). "Preparation of CoFe alloy nanoparticles with tunable electromagnetic wave absorption performance," *J. Magn. Magn. Mater.* 321(22), 3702-3705.

Guan, H., Liu, S., Duan, Y., and Zhao, Y. (2007). "Investigation of the electromagnetic characteristics of cement based composites filled with EPS," *Cement Concrete Comp*. 29(1), 49-54.

Han, Z., Li, D., Wang, H., Liu, X. D., Li, J., Geng, D. Y., and Zhang, Z. D. (2009). "Broadband electromagnetic-wave absorption by FeCo/C nanocapsules," *Appl. Phys. Lett.* 95(2), 023114-023114-3.

Hibbins, A. P., Murray, W. A., Tyler, J., Wedge, S., Barnes, W. L., and Sambles, J. R. (2006). "Resonant absorption of electromagnetic fields by surface plasmons buried in a multilayered plasmonic nanostructure," *Phys. Rev. B.* 74(7), 73401-73408.

Hou, C., Li, T., Zhao, T., Liu, L., and Zhang, W. (2013). "Electromagnetic wave absorbing properties of multi-wall carbon nanotube/Fe_3O_4 hybrid materials," *New Carbon Mater*. 28(3), 184-190.

Ismail, M. S., and Waliuddin, A. M. (1996). "Effect of rice husk ash on high strength concrete," *Constr. Build Mater.* 10(7), 521-526.

Kim, S. S., Kim, S., Ahn, J. M., and Kim, K. H. (2004). "Magnetic and microwave absorbing properties of Co–Fe thin films plated on hollow ceramic microspheres of low density," *J. Magn. Magn. Mater.* 271(1), 39-45.

Kord, B. (2011). "Nanofiller reinforcement effects on the thermal, dynamic mechanical, and morphological behavior of HDPE/rice husk flour composites," *BioResources* 6(2), 1351-1358.

Liu, Q., Zhang, D., and Fan, T. (2004). "Electromagnetic wave absorption properties of porous carbon/Co nanocomposites," *Appl. Phys. Lett.* 93(1), 013110-013110-3

Luo, X., and Chung, D. D. L. (1999). "Electromagnetic interference shielding using continuous carbon-fiber carbon-matrix and polymer-matrix composites," *Compos. B: Eng*. 30(3), 227-231.

Lv, S., Chen, X., Ye, Y., Yin, S., Cheng, J., and Xia, M. (2009). "Rice hull/$MnFe_2O_4$ composite: Preparation, characterization and its rapid microwave-assisted COD removal for organic wastewater," *J. Hazard. Mater.* 171(1-3), 634-639.

Memon, S. A., Shaikh, M. A., and Hassan, A. (2011). "Utilization of rice husk ash as viscosity modifying agent in self compacting concrete," *Constr. Build Mater*. 25(2), 1044-1048.

Moučka, R., Lopatin, A. V., Kazantseva, N. E., Vilčáková, J., and Sáha, P. (2007). "Enhancement of magnetic losses in hybrid polymer composites with MnZn-ferrite and conductive fillers," *J. Mater. Sci.* 42(22), 9480-9490.

Nornikman, H., Soh, P. J., Azremi, A. H., Wee, F. H., and Malek, M. F. (2009). "Investigation of an agricultural waste as an alternative material for microwave absorbers," *PIERS 2009 Moscow Vols. I and II, Proceedings*, pp. 1287-1291.

Nornikman, H., Malek, F., Soh, P. J., Azremi, A. A. H., Wee, F. H., and Hasnain, A. (2010). "Parametric studies of the pyramidal microwave absorber using rice husk," *Progress in Electromagnetics Research-Pier.* 104, 145-166.

Park, B., Wi, S. G., Lee, K. H., Singh, A. P., Yoon, T., and Kim, Y. S. (2003). "Characterization of anatomical features and silica distribution in rice husk using microscopic and micro-analytical techniques," *Biomass Bioener.* 25(3), 319-327.

Park, K. Y., Lee, S. E., Kim, C. G., and Han, J. H. (2006). "Fabrication and electromagnetic characteristics of electromagnetic wave absorbing sandwich structures," *J. Compos Sci Technol*. 66(3-4), 576-584.

Rahman, M. R., Islam, M. N., Huque, M. M., Hamdan, S., and Ahmed, A. S. (2010). "Effect of chemical treatment on rice husk (RH) reinforced polyethylene (PE) composites," *BioResources* 5(2), 854-869.

Roy, P. K., and Bera, J. (2009). "Electromagnetic properties of samarium-substituted NiCuZn ferrite prepared by auto-combustion method," *J. Magn. Magn. Mater.* 321(4), 247-251.

Ruckenstein, E., and Park, J. S. (1991). "The electromagnetic interference shielding of polypyrrole impregnated conducting polymer composites," *Polym. Compos*. 12(4), 289-292.

Sievenpiper, D., Zhang, L., Broas, R. F. J., Alexopolous, N. G., and Yablonovitch, E. (1999). "High-impedance electromagnetic surfaces with a forbidden frequency band," *IEEE T. Microw. Theory* 47(11), 2059-2074.

Suigimoto, S., Haga, K., Kagotani, T., and Inomata, K. (2005). "Microwave absorption properties of Ba M-type ferrite prepared by a modified coprecipitation method," *J. Magn. Magn. Mater.* 290-291, 1188-1191.

Wu, Z., Li, M., Hu, Y., Wang, Z., Yin, Y., Chen, Y., and Zhou, X. (2011). "Electromagnetic interference shielding of carbon nanotube macrofilms," *Scripta. Mater*. 64(9), 809-812.

Yalçın, N., and Sevinç, V. (2000). "Studies of the surface area and porosity of activated carbons prepared from rice husks," *Carbon* 38(4), 1943-1945.

Yang, Y., and Gupta, M. C. (2005). "Novel carbon nanotube-polystyrene foam composites for electromagnetic interference shielding," *Nano. Lett.* 5(11), 2131-2134.

Yoshida, S., Mitsuharu, S., Sugawara, E., and Shimada, Y. (1999). "Permeability and electromagnetic-interference characteristics of Fe-Si-Al alloy flakes polymer composite," *J. Appl. Phys.* 85(8), 4636-4638.

Zhao, D., Li, X., and Shen, Z. (2009). "Preparation and electromagnetic and microwave absorbing properties of Fe-filled carbon nanotubes," *J. Alloy. Compd.* 471(1-2), 457-460.

Zhou, J., He, J., Wang, T., Sun, D., Ding, S., Zhao, J., and Wu, S. (2010). "Direct incorporation of magnetic constituents within ordered mesoporous carbon-silica nanocomposites for highly efficient electromagnetic wave absorbers," *J. Phys. Chem. C* 114(17), 7611-7617.

Article submitted: December 13, 2013; Peer review completed: Feb. 20, 2014; Revised version received and accepted: March 6, 2014; Published: March 11, 2014.